IEEE Access
Multidisciplinary | Rapid Review | Open Access Journal

Received 5 October 2022, accepted 4 November 2022, date of publication 9 November 2022, date of current version 15 November 2022.

Digital Object Identifier 10.1109/ACCESS.2022.3220770

METHODS

Active Cross Pre-Compensation Decoupling Control of X-Y Linear Motor Platform Based on Contour Error Analysis Model

RONGKUN WANG, ZHIBIN CHEN, QUANKAI DU, ZUOCHAO YU, WENJIE HUANG, AND XINHUA GUO

College of Information Science and Engineering, Huaqiao University, Xiamen 361000, China

Corresponding author: Rongkun Wang (wangrongkun@hqu.edu.cn)

This work was supported in part by the Youth Innovation Foundation of Xiamen under Grant 3502Z202006016, and in part by the Fundamental Research Funds for the Central University of Huaqiao University under Grant ZQN-908.

ABSTRACT To improve the position accuracy of the X-Y linear motor motion platform, this paper derives a contour error analysis model (CEAM) and proposes an active cross pre-compensation decoupling controller (ACPDC). Three major factors affect the tracking performance of the X-Y motion platform are obtained from the derived CEAM: uniaxial-axis subsystem performance, dynamic compatibility between multiple axes, and disturbances. CEAM also shows that better contour control can be achieved by combining the unified modeling idea. Therefore, the ACPDC proposed in this paper integrates the inter-axis controller and single-axis subsystem by establishing a unified control law that combines active pre-compensation control with linear active disturbance rejection control. The theoretical analysis based on CEAM shows that ACPDC achieves improvements in the above three aspects. Finally, experimental results on an X-Y linear motor platform support the CEAM analysis that ACPDC has better contouring performance than other multi-axis controllers. Compared with these controllers, ACPDC has the best system robustness and uniaxial tracking performance.

INDEX TERMS Contour error, contour error analysis model, X-Y linear motor platform, active cross pre-compensation decoupling controller.

I. INTRODUCTION

With the continuous improvement of precision product quality, the precision requirements for X-Y linear motor motion platforms also increase [1]. As a multi-axis motor system, how to coordinate contour motion of multiple axes is one of the important studies. Contour error is an important index to evaluate contour performances in motion control [2], which is defined as the shortest distance between the actual motion position and contour reference. Conventional PID controllers do not perform well in load-disturbing coupled system [3]. To effectively decrease contour error, researchers have proposed many control strategies. And this paper briefly divides them into the indirect method and direct method according to differences in controlled objects.

The indirect method is to optimize the uniaxial controller to reduce uniaxial tracking error as a way to indirectly promote the contour tracking accuracy, such as feedforward control. Friction compensation control [4] and zero-phase error tracking control [5] are commonly used indirect methods, which respectively eliminate uniaxial tracking error caused by friction disturbance and system delay. Beside PID controller, advanced strategies, e.g., model-free control [6] and predictive control [7], can also achieve better tracking performances. The disturbance observer [8] added to the feedback-loop reduces the influences of uncertainty factors, which also improves uniaxial performances. However, the indirect method is limited by the performances of the controller and does not take into account dynamic

The associate editor coordinating the review of this manuscript and approving it for publication was Mohammad Alshabi.

incompatibility between multiple axes, so the direct method is proposed.

The direct method refers to inter-axis control strategies, which directly works on contour motion. It is the main solution to coordinate dynamic compatibility between multiple axes and reduce contour error, such as cross-coupling control (CCC) [9]. Nevertheless, CCC obtains contour error by complex approximate calculations, which have an impact on the contour accuracy. Therefore, CCC requires a better compensation controller to make up for contour error. On the one hand, advanced strategies have introduced into the compensation controllers, including robust control [10], iterative learning control [11], and neural network [12], to replace the conventional PID compensation controller. On the other hand, a lot of achievements have been made in the research of gain structure. Variable-gain control [13] and model predictive control [14] are adopted instead of the conventional fixed gain structure to obtain high-precision contour control for tracking different curves. Moreover, the feedback pre-compensation structure [15] is incorporated in CCC to enable the fast synchronization of multiple axes and thus promote the contour tracking precision. Although high-performance contour control can be achieved through various aspects (e.g., uniaxial subsystem performances, dynamic compatibility between multiple axes [16], and disturbances [17]), more attention has focused on facilitating partial controllers. In other words, these controllers can improve system performances, but do not take into account the intrinsic relations between these factors and contour error, such as the coupling among different factors. This leads to a complex contour structure and one-dimensional research. The main reason for this is that few studies have explored the essence of contour error. Therefore, it is necessary to derive a multi-dimensional unified analysis model, which can analyze the essence of contour error. Also, it can help researchers design and verify controllers from an overall perspective to make improvements with simple structures.

To solve the problems in the indirect and direct methods described above, this paper deduces a contour error analysis model (CEAM) for an X-Y motion platform with an inter-axis controller. Specifically, it can be qualitatively proved from CEAM that contour error is generated by three critical factors: uniaxial subsystem performances, dynamic compatibility between multiple axes, and disturbances. Meanwhile, CEAM provides a quantitative analysis of contour error sensitivity and predicts contour performances with the actual parameters. Then, based on the conclusion of CEAM and the idea of unified modeling [18], the uniaxial subsystem and the inter-axis controller as a whole, this paper designs the active cross pre-compensated decoupling control (ACPDC) strategy. This paper first proposes active pre-compensation control (APC) to enhance the coupling level between the biaxial systems and designs the second-order linear active disturbance rejection controller (LADRC) to suppress disturbances. Then, by establishing a unified control law to combine APC and LADRC, ACPDC with a double closed-loop contour compensation structure is built. Theoretically, CEAM demonstrates the system performances improvement of ACPDC in all three aspects. Experiments show the contour performances are consistent with the CEAM analysis. Compared with other conventional strategies [9], ACPDC not only directly decreases contour error but also promotes robustness and uniaxial subsystem performances to indirectly increase contour performances.

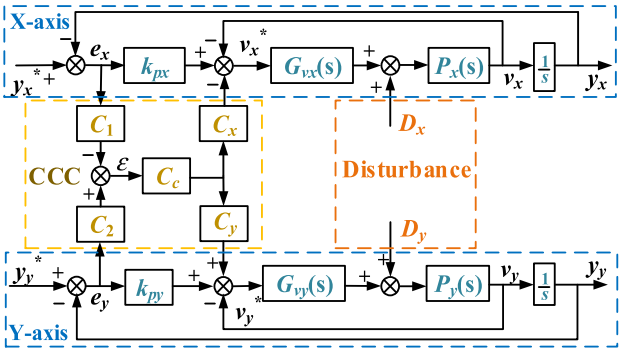

FIGURE 1. The X-Y linear motion system based on CCC. where C_1 and C_2 represent the contour error estimation coefficients of X-axis and Y-axis, ε is the contour error, C_i is the cross-coupling compensation gain coefficient, C_c is the contour compensation gain coefficient, k_{pi} is the proportional coefficient of position-loop, y_i^*, y_i represents the reference signal and output signal respectively, e_i is the uniaxial tracking error, D_i denotes the total disturbance signal, $G_{vi}(s)$ is the proportional-integral controller of velocity-loop, $P_i(s)$ represents the velocity-loop controlled object. i = x, y, denoting X-axis and Y-axis respectively.

II. CONTROUR ERROR ANALYSIS MODEL

A. CROSS-COUPLING CONTROL

The inter-axis controller is a conventional strategy used in contour motion studies to adjust dynamic compatibility and improve contour accuracy. Fig. 1 shows the structure of an X-Y linear motion system based on CCC.

Gvi(s) can be expressed as

$$G_{vi}(s) = k_{vpi} + \frac{k_{vki}}{s} \tag{1}$$

where k_{vpi} is the proportionality coefficient of the velocity-loop, k_{vki} is the integration coefficient of the velocity-loop.

The current-loop can be regarded as a unit transfer function, so P_i can be represented as

$$P_i(s) = \frac{1}{M_i s + B_i} \tag{2}$$

where B_i is the viscous friction coefficient, M_i is the total mass of the mover and load.

The uniaxial position tracking error is

$$e_i = y_i^* - y_i \tag{3}$$

The contour error estimation formula [8] is

$$\varepsilon = -C_1 e_x + C_2 e_y \tag{4}$$

The error gain of linear trajectories can be obtained by the Taylor first-order expansion [19]

$$\begin{cases} C_1 = sin\theta \\ C_2 = cos\theta \end{cases} \tag{5}$$

where θ is the angle between the tangent line at the reference position and the X-axis.

The CCC compensations for uniaxial subsystems are

$$\begin{cases} \varepsilon_x = C_x C_c \varepsilon \\ \varepsilon_y = C_y C_c \varepsilon \end{cases} \tag{6}$$

where ε_x and ε_y are the compensation from CCC to the X-axis and Y-axis respectively.

B. CONTOUR ERROR ANALYSIS MODEL

Although the relation between contour error and uniaxial tracking error can be seen in (4), the coupling relation of other factors cannot be explored in detail. Therefore, CEAM is built to deal with this problem from both qualitative and quantitative perspectives in this section. The CEAM modeling process can be divided into four steps as follows:

Step 1: The reference signal independently exerts

Take the X-axis as an example, a transfer function for the position-loop controlled object H_x is

$$H_x(s) = \frac{G_{vx}(s) P_x(s)}{1 + G_{vx}(s) P_x(s)} \frac{1}{s} = \frac{G_{vx}(s) P_x(s)}{s + G_{vx}(s) P_x(s) s} \tag{7}$$

The relation between y_x^* and y_x is

$$\left[\left(y_x^* - y_x\right) k_{px} - \varepsilon_1 C_c C_x\right] H_x(s) = y_x \tag{8}$$

Step 2: The disturbances signal independently exerts

Under the action of D_x, y_x is

$$\left[\left(-\varepsilon_1 C_c C_x - y_x k_{px} - v_x\right) G_{vx}(s) + D_x\right] P_x(s) = s y_x \tag{9}$$

Step 3: Calculate the uniaxial tracking error

Adding (8) to (9), under combined action of y_{x*} and D_x, y_x is

$$\begin{aligned} y_x = & \frac{k_{px} H_x(s) y_x^* - C_x C_c H_x(s) \varepsilon_1}{1 + H_x(s) k_{px}} \\ & - \frac{C_x C_c G_{vx}(s) P_x(s) \varepsilon_1 - D_x P_x(s)}{s + G_{vx}(s) k_{px} P_x + s G_{vx}(s) P_x(s)} \end{aligned} \tag{10}$$

Then, the X-axis tracking error e_x is

$$\begin{aligned} e_x = y_x^* - y_x = & \frac{y_x^* + C_x C_c H_x(s) \varepsilon_1}{1 + H_x(s) k_{px}} \\ & + \frac{C_x C_c G_{vx}(s) P_x(s) \varepsilon_1 - D_x P_x(s)}{s + G_{vx}(s) k_{px} P_x(s) + s G_{vx}(s) P_x(s)} \end{aligned} \tag{11}$$

Similarly, the Y-axis tracking error e_y can be obtained by the above three steps,

$$\begin{aligned} e_y = y_y^* - y_y = & \frac{y_y^* - C_y C_c H_y(s) \varepsilon_1}{1 + H_y(s) k_{py}} \\ & - \frac{C_y C_c G_{vy}(s) P_y(s) \varepsilon_1 + D_y P_y(s)}{s + G_{vy}(s) k_{py} P_y(s) + s G_{vy}(s) P_y(s)} \end{aligned} \tag{12}$$

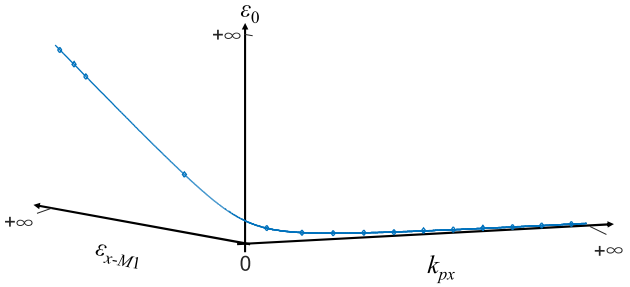

FIGURE 2. The indirect method characteristic curve.

where

$$H_y(s) = \frac{G_{vy}(s) P_y(s)}{1 + G_{vy}(s) P_y(s)} \frac{1}{s} = \frac{G_{vy}(s) P_y(s)}{s + G_{vy}(s) P_y(s) s} \tag{13}$$

Step 4: CEAM modeling

Substituting (11) and (12) into (4), then CEAM for the biaxial coupled system (CEAM-CCC) is

$$\begin{aligned} \varepsilon_1 &= -\frac{y_x^* b_1 e_1}{a_1 b_1 + 2 b_1 c_1 + 2 a_1 d_1} + \frac{y_y^* a_1 f_1}{a_1 b_1 + 2 b_1 c_1 + 2 a_1 d_1} \\ &= \frac{g_1 b_1}{a_1 b_1 + 2 b_1 c_1 + 2 a_1 d_1} - \frac{h_1 a_1}{a_1 b_1 + 2 b_1 c_1 + 2 a_1 d_1} \\ &= -\varepsilon_{x-\mathrm{M2}} + \varepsilon_{y-\mathrm{M2}} + \varepsilon_{xd-\mathrm{M2}} - \varepsilon_{yd-\mathrm{M2}} \end{aligned} \tag{14}$$

$$\begin{cases} a_1 = s + G_{vx}(s) k_{px} P_x(s) + s G_{vx}(s) P_x(s) \\ b_1 = s + G_{vy}(s) k_{py} P_y(s) + s G_{vy}(s) P_y(s) \\ c_1 = C_c C_x C_1 G_{vx}(s) P_x(s) \\ d_1 = C_c C_y C_2 G_{vy}(s) P_y(s) \\ e_1 = \left(1 + G_{vx}(s) P_x(s)\right) s C_1 \\ f_1 = \left(1 + G_{vy}(s) P_y(s)\right) s C_2 \\ g_1 = D_x P_x(s) C_1 \\ h_1 = D_y P_y(s) C_2 \end{cases} \tag{15}$$

where ε_{x-M2}, ε_{y-M2}, ε_{xd-M2}, and ε_{yd-M2} are the X-axis tracking error, Y-axis tracking error, X-axis disturbances, and Y-axis disturbances in contour error under the conventional direct method, respectively.

Except for CCC, the structure of the biaxial uncoupled system is the same as Fig. 1. It implies that CEAM for the biaxial uncoupled system (CEAM-PID) is a special case of (14), where $C_x = C_y = 0$ and $C_c = C_1 = C_2 = 1$ is satisfied. CEAM-PID can be rewritten as

$$\begin{aligned} \varepsilon_0 &= \frac{y_x^* e_1}{a_1} + \frac{y_y^* f_1}{b_1} + \frac{g_1}{a_1} + \frac{h_1}{b_1} \\ &= -\varepsilon_{x-\mathrm{M1}} + \varepsilon_{y-\mathrm{M1}} + \varepsilon_{xd-\mathrm{M1}} - \varepsilon_{yd-\mathrm{M1}} \end{aligned} \tag{16}$$

According to CEAM-CCC and CEAM-PID, it can be proved that contour error is generated by three factors:

(1) *Uniaxial subsystem performances*: a_1, b_1, e_1, and f_1 are composed of uniaxial controller parameters.

As shown in Fig. 2, the larger k_{px}, the better the contour performances. When the uniaxial controllers' gain reaches infinite, zero-error contour tracking is achieved, i.e., $\varepsilon_0 = 0$. In the mean-time, ε_{xd-M1} and ε_{yd-M1} are also equal to

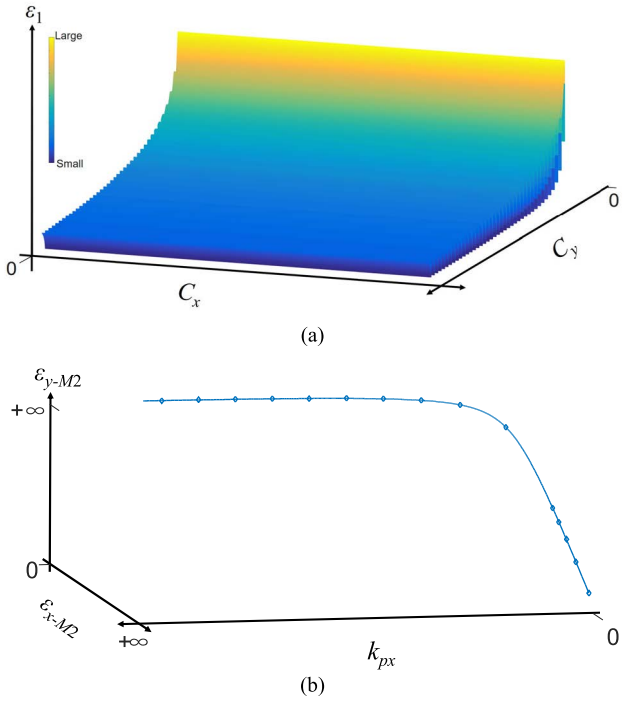

FIGURE 3. The direct method characteristic curve. (a) Relation between contour error and CCC, (b) The disadvantage of the direct method.

zero, which implies that the effects of disturbances on contour motion is reduced.

(2) *Biaxial dynamic compatibility*: c_1, d_1, e_1, f_1, g_1, and h_1 all include inter-axis controller parameters.

When biaxial systems are identical, i.e., $a_1 = b_1$, $c_1 = d_1$, $e_1 = f_1$, and $g_1 = h_1$, they have the same dynamic characteristics. This means that $\varepsilon_{x-M2} = \varepsilon_{y-M2}$, $\varepsilon_{xd-M2} = \varepsilon_{yd-M2}$, and the contour error is zero, but it is difficult to satisfy this situation. So based on CEAM to compare performances of the uncoupled system and coupled system. If they have same uniaxial controllers and parameters, the coupled system will have better contour performances. Above phenomenon is further proved in Fig. 3(a), where the uncoupled system ($C_x = C_y = 0$) has a large contour error than the coupled system ($C_x \neq 0$, $C_y \neq 0$). Thus, the inter-axial controller becomes a new strategy to reduce contour error without increasing the controllers' gains. Nevertheless, the controllers of multiple axes are coupled to each other in (14). As shown in Fig. 3(b), while increasing the X-axis parameters will reduce ε_{x-M2}, it also causes ε_{y-M2} to increase. This is not conducive to adjusting dynamic incompatibility and reducing contour error.

(3) *Disturbances*: both g_1 and h_1 include disturbance parameters.

According to CEAM-CCC, the disturbance components are hidden in e_x and e_y, and they will be next fed into the contour error estimation model ε_1. Then, ε_x and ε_y are compensated to the other axes by CCC, which will produce additional error.

There are some differences between CEAM proposed in this paper and [19]. Particularly speaking, except for the qualitative explore, CEAM also focuses on quantitative analysis. On the one hand, CEAM discusses the action mechanism and coupling of contour error factors. On the other hand, CEAM is used to study controllers' defects before design and to verify its improvements. Thus, CEAM can summarize the contour performances as follows:

Conclusion 1: By optimizing the uniaxial controllers, the uniaxial error and disturbance error can be reduced to promote the contour accuracy indirectly.

Conclusion 2: The uniaxial error and contour error are formed into a coupling relation. It means that optimal control for the multi-axis system cannot be achieved by improving one of them.

Conclusion 3: Disturbances should be suppressed in the generated axes, otherwise they will negatively affect the inter-axis controller and other axes.

In conclusion, if a unified controller is designed by integrating the indirect and direct methods, optimized contour performances can be obtained.

III. ACTIVE CROSS PRE-COMPENSATION DECOUPLING CONTROLLER

A. CONTROLLER DESIGN

1) ACTIVE PRE-COMPENSATION CONTROLLER

Because of the limited gain range of the uniaxial controller noted in conclusion 1, an inter-axis controller was designed to further improve tracking performance. With a high-precision contour error estimation model, controllers can get more accurate information. And the advanced compensation controller is adopted to promote the convergence speed and steady-state precision of contour tracking. However, these strategies easily lead to complex inter-axis controllers and neglect disturbances.

As described in conclusion 2, the contour performances are improved when the coupling level is further enhanced. And the compensation mode of CCC is an active adjusting speed control for motors. In other words, it improves the tracking performance by actively accelerating the change of motor speed. Therefore, APC is proposed by combining the coupling characteristic with the active variable speed characteristic. Compared with (14), APC makes minor adjustments to coupling terms c_1 and d_1 in CEAM-CCC

$$\begin{cases} c_2 = C_1 C_c G_{vx}(s) P_x(s) \left(X_x + C_x\right) \\ d_2 = C_2 C_c G_{vy}(s) P_y(s) \left(X_y + C_y\right) \end{cases} \tag{17}$$

where X_x and X_y are the active correction coefficient of the X-axis and Y-axis respectively.

So CEAM for APC (CEAM-APC) is

$$\begin{aligned} \varepsilon_2 &= -\frac{y_x^* C_1 b_1 e_1}{a_1 b_1 + 2 b_1 c_2 + 2 a_1 d_2} + \frac{y_y^* C_2 a_1 f_1}{a_1 b_1 + 2 b_1 c_2 + 2 a_1 d_2} \\ &\quad + \frac{g_1 b_1}{a_1 b_1 + 2 b_1 c_2 + 2 a_1 d_2} - \frac{h_1 a_1}{a_1 b_1 + 2 b_1 c_2 + 2 a_1 d_2} \\ &= -\varepsilon_{x-\mathrm{A}} + \varepsilon_{y-\mathrm{A}} + \varepsilon_{xd-\mathrm{A}} - \varepsilon_{yd-\mathrm{A}} \end{aligned} \tag{18}$$

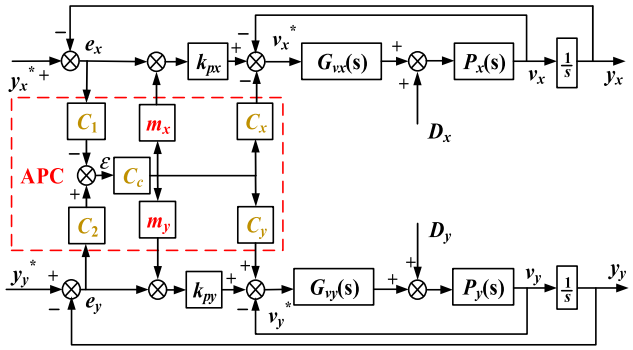

FIGURE 4. The X-Y linear motion system based on APC.

When both X_x and X_y are greater than 0 in (17), ε_2 is smaller than ε_1 in (18) and (14). Also, comparing disturbances components in CEAM-CCC and CEAM-APC, the dual-channel structure provides better suppression for disturbances.

In addition to the above optimization aspects, it is necessary to further discuss the location of the active pre-compensation channel and analyze its effect on a uniaxial subsystem. The structure of a biaxial system based on APC is shown in Fig. 4.

The active pre-compensation coefficients m_x and m_y of X-axis and Y-axis are

$$\begin{cases} X_x = m_x k_{px} \\ X_y = m_y k_{py} \end{cases} \tag{19}$$

For a uniaxial subsystem, the position-loop is the outermost loop of a three-loop cascade structure. Also, it provides reference signals for the inner loops, e.g., the velocity-loop and current-loop. Therefore, as described in Fig.4, the active pre-compensation channel placed in the position-loop can contribute to the uniaxial subsystem robustness and position performances than other loops.

2) LINEAR ACTIVE DISTURBANCE REJECTION CONTROLLER

Compared to a permanent magnet synchronous motor, PMLSM eliminates intermediate transmission links. The thrusts and disturbances are directly exerted on PMLSM without any buffer, which will cause a decline of the uniaxial performances. When the controlled objects are converted into multiple axes, these disturbances are amplified to decrease motor performances. Nevertheless, reducing the effects of disturbances is not suitable for model-based method because disturbances are strongly random, such as friction resistance and load variation. Therefore, LADRC is introduced into motion systems to separate and compensate for disturbances in this research, which is a model-free method.

PMLSM electromagnetic thrust equation is

$$F_{em} = \frac{3\pi n_p}{2\tau}\psi_m i_q \tag{20}$$

where F_{em} is the electromagnetic thrust, n_p is the number of polar-pairs, τ denotes the distance between poles, ψ_m is the permanent magnet flux linkage, i_q is the q-axis current.

PMLSM motion equation is

$$M\dot{v} = F_{em} - F_l - Bv \tag{21}$$

where v is the mover running speed, F_l is the load torque.

By combining (20) and (21), the mover position p and v are changed to state variables as

$$\begin{cases} \dot{p} = v \\ \dot{v} = b_L i_q + a_L(t) \end{cases} \tag{22}$$

where $b_L = (3\pi n_p \psi_m)/(2\tau M)$, $a_L(t) = (-F_l - f)/M - k_L v$, $k_L = B/M$, f is the unmolded disturbances.

State variables z_1 and z_2 are defined as the estimated values of p and v, and the extended state variable $z_3 = a_L(t)$. Then a LESO is created as

$$\begin{cases} \dot{z}_1 = z_2 - \beta_1(z_1 - p) \\ \dot{z}_2 = z_3 - \beta_2(z_1 - p) + b_L u \\ \dot{z}_3 = -\beta_3(z_1 - p) \end{cases} \tag{23}$$

The observer estimation errors e_{c1}, e_{c2}, and e_{c3} are defined as

$$\begin{cases} e_{c1} = z_1 - p \\ e_{c2} = z_2 - v \\ e_{c3} = z_3 - a_L(t) \end{cases} \tag{24}$$

The system state variables errors $\dot{e}_{c1}$, $\dot{e}_{c2}$, and $\dot{e}_{c3}$ are

$$\begin{cases} \dot{e}_{c1} = -\beta_1 e_{c1} + e_{c2} \\ \dot{e}_{c2} = -\beta_2 e_{c1} + e_{c3} \\ \dot{e}_{c3} = -\beta_3 e_{c1} - k_L e_{c3} + a_L \end{cases} \tag{25}$$

Extract the characteristic equation of (25) is

$$\lambda(s) = \lambda^3 + (k_L + \beta_1)\lambda^2 + (k_L\beta_1 + \beta_2)\lambda + k_L\beta_2 + \beta_3 \tag{26}$$

According to the Lyapunov stability law, if the observer error convergence is guaranteed, all eigenvalues should be on the left half of coordinate axis. In the meantime, according to the bandwidth-based parameters tuning idea [21], the ideal characteristic polynomial of (25) is

$$\lambda(s) = (\lambda + \omega_o)^3 \tag{27}$$

Combining (26) and (27), it can get

$$\begin{cases} \beta_1 = 3\omega_o - k_L \\ \beta_2 = 3\omega_o^2 - k_L\beta_1 \\ \beta_3 = \omega_o^3 - k_L\beta_2 \end{cases} \tag{28}$$

where ω_o is the observer bandwidth.

The estimation of real-time state variables and total disturbances can be achieved by selecting appropriate observer gains based on (28). The linear feedback control law is

$$u = \frac{u_0 - z_3}{b_L} = \frac{K_{pL}(P^* - z_1) - K_{dL}z_2 - z_3}{b_L} \tag{29}$$

where K_{pL} and K_{dL} are the proportional gain of z_1 and z_2, $K_{pL} = \omega_c^2$, $K_{dL} = 2\omega_c\xi$. ωc is the system bandwidth, ξ denotes the system damping ratio.

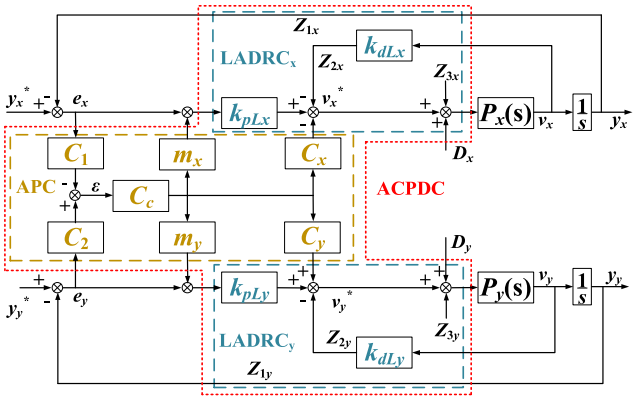

FIGURE 5. The X-Y linear motion system based on ACPDC.

The system variables shown in (22) can be rewritten as

$$\begin{cases} \dot{p} = v \\ \dot{v} = u \\ y = p \end{cases} \tag{30}$$

In (22) and (30), when the observation error is close to zero, LESO can achieve the separation of the disturbance signals from feedback signals. Then disturbances will be compensated by LADRC.

3) ACTIVE CROSS PRE-COMPENSATION DECOUPLING CONTROLLER

Although LADRC improves the uniaxial subsystem robustness, there is an additional problem when APC and LADRC are applied together. Specifically, if compensations generated by APC is directly added to a uniaxial subsystem, it will be estimated and compensated by LADRC as a total disturbance, resulting in compensation failure or even control mismatch. To deal with the above problems, APC and LADRC will be combined to design ACPDC through the unified control law. According to (4), the control law (29) will be converted to (31) as

$$u = \frac{K_{pL}(y^* - z_1 + m_i C_c \varepsilon) - K_{dL} z_2 + C_i C_c \varepsilon - z_3}{b_L} \tag{31}$$

The estimated contour error is fed into each axis and used to modify the reference signal. Then take the coupling control value as a pre-compensation for the path instruction. In the meantime, to improve dynamic compatibility between multiple axes, the feedforward signals obtained by multiplying the couple control values with specific gains are input to the uniaxial subsystem. Fig. 5 presents the structure of a biaxial system using ACPDC under ideal conditions.

The uniaxial system stability can be ensured by selecting appropriate parameters according to (28) and (29) so that all poles are on the left half of coordinate axis. Because the coupling compensation has an impact on the system stability (e.g., X-axis), substituting (31) into (22) obtains (32).

$$\begin{cases} \dot{p}_x = v_x \\ \dot{v}_x = K_{pLx}(y_x^* - z_{1x} + m_x C_c \varepsilon) - K_{dLx} z_{2x} \\ \qquad + C_x C_c \varepsilon - z_{3x} + a_{Lx}(t) \end{cases} \tag{32}$$

When contour error is close to zero, (31) can be expressed as

$$u_x = K_{pLx}(e_x + m_x C_c \varepsilon) - K_{dLx} z_{2x} + C_x C_c \varepsilon \tag{33}$$

Combine (5), (6), and (7), defining that

$$\begin{cases} h_{1x} = (K_{pLx} - K_{pLx} m_x C_1 C_c - C_x C_1 C_c) \\ h_{2x} = C_2 C_c (K_{pLx} m_x + C_x) \end{cases} \tag{34}$$

Then (33) can be converted to

$$u_x = h_{1x} e_x - K_{dLx} z_2 + h_{2x} e_y \tag{35}$$

In (29) and (35), h_{1x} will lead to an enhancement of e_x, which corresponds to an increase in w_c of the uniaxial controller. At the same time, $0 < \xi < 1$ is satisfied in the second-order underdamped system, so $w_c > \xi w_c$. Thus, based on the relation between poles and parameters, the system poles get closer to the imaginary axis as w_c increases. Therefore, h_1 and h_2 should be determined by the performance requirements of motion system.

B. CEAM OF ACPDC

The multi-axis control structure based on ACPDC as shown in Fig. 5. To further analysis the performances of ACPDC, combine the four-step CEAM modelling method to build CEAM for ACPDC (CEAM-ACPDC) is

$$\begin{aligned} \varepsilon_3 &= -\frac{y_x^* b_3 e_3}{a_3 b_3 + 2 b_3 c_3 + 2 a_3 d_3} + \frac{y_y^* a_3 f_3}{a_3 b_3 + 2 b_3 c_3 + 2 a_3 d_3} \\ &\quad + \frac{g_3 b_3}{a_3 b_3 + 2 b_3 c_3 + 2 a_3 d_3} - \frac{h_3 a_3}{a_3 b_3 + 2 b_3 c_3 + 2 a_3 d_3} \\ &= -\varepsilon_{x-\mathrm{M3}} + \varepsilon_{y-\mathrm{M3}} + \varepsilon_{xd-\mathrm{M3}} - \varepsilon_{yd-\mathrm{M3}} \end{aligned} \tag{36}$$

$$\begin{cases} a_3 = s + K_{pLx} P_x(s) + s K_{dLx} P_x(s), \\ \qquad e_3 = (1 + K_{dLx} P_x(s))\, s C_1 \\ b_3 = s + K_{pLy} P_y(s) + s K_{dLy} P_y(s), \\ \qquad f_3 = \left(1 + K_{dLy} P_y(s)\right) s C_2 \\ c_3 = C_1 C_c P_x(s) \left(m_x K_{pxL} + C_x\right), \\ \qquad g_3 = (D_x - Z_{3x})\, P_x(s) C_1 \\ d_3 = C_1 C_c P_y(s) \left(m_y K_{pyL} + C_y\right), \\ \qquad h_3 = \left(D_y - Z_{3y}\right) P_y(s) C_2 \end{cases} \tag{37}$$

Firstly, the Routh criterion is used to analyze the stability of the ACPDC-based biaxial system. Extracting the characteristic equation from (36) is

$$F(s) = L_1 s^4 + L_2 s^3 + L_3 s^2 + L_4 s + L_5 \tag{38}$$

TABLE 1. The rouse list.

s^4	L_1	L_3	L_5
s^3	L_2	L_4	0
s^2	L_6	L_5	
s^1	L_7	0	
s^0	L_5		

$$\begin{cases} L_1 = M_x M_y \\ L_2 = \left(K_{dLy} + B_y\right) M_x + \left(K_{dLx} + B_x\right) M_y \\ L_3 = B_x K_{dLy} + B_y K_{dLx} + M_x K_{pLy} + M_y K_{pLx} \\ \quad + K_{dLx} K_{dLy} + B_x B_y + 2M_x c_1 c_c c_x + 2M_x c_2 c_c c_y \\ \quad + 2M_y c_1 c_c K_{pLx} m_x + 2M_x c_2 c_c K_{pLy} m_y \\ L_4 = B_x K_{pLy} + B_y K_{pLx} + K_{dLx} K_{pLy} \\ \quad + K_{dLy} K_{pLx} + 2B_y c_1 c_c c_x + 2B_x c_2 c_c c_y \\ \quad + 2c_1 c_c c_x K_{dLy} + 2c_2 c_c c_y K_{dLx} + 2B_y c_1 c_c K_{pLx} m_x \\ \quad + 2B_x c_2 c_c K_{pLy} m_y + 2c_1 c_c K_{dLy} K_{pLx} m_x \\ \quad + 2c_2 c_c K_{dLx} K_{pLy} m_y \\ L_5 = K_{pLx} K_{pLy} + 2c_1 c_c c_x K_{pLy} + 2c_2 c_c c_y K_{pLx} \\ \quad + 2c_1 c_c K_{pLx} K_{pLy} m_x + 2c_2 c_c K_{pLx} K_{pLy} m_y \end{cases} \tag{39}$$

Organize (38) into the Rouse list, as shown in Table 1

$$\begin{cases} L_6 = \dfrac{(L_2 L_3 - L_1 L_4)}{L_2} \\ L_7 = \dfrac{(L_6 L_4 - L_2 L_5)}{L_6} \end{cases} \tag{40}$$

Since the ACPDC parameters are all real numbers and greater than zero, coefficients in Table 1 satisfy

$$\begin{cases} L_1 > 0 \\ L_2 > 0 \\ L_6 > 0 \\ L_7 > 0 \\ L_5 > 0 \end{cases} \tag{41}$$

According to the analysis in (41), the stability of the ACPDC-based biaxial motion system can be determined.

Secondly, the system robustness is explored. If LESO reaches the ideal observation state

$$z_{3x} = D_x, z_{3y} = D_y \tag{42}$$

When (42) is substituted into (36), both ε_{xd-M3} and ε_{yd-M3} are equal to zero. It means that the system disturbances are eliminated to avoid the transmission of inter-axial disturbances and to reduce contour error.

However, since the actual control system is non-idealized, it is necessary to consider a case where disturbance components are not eliminated completely. The closed-loop characteristic curves of the system response are drawn based on CEAM-PID (14), CEAM-CCC (16), and CEAM-ACPDC (36), respectively, as shown in Fig. 6.

In Fig. 6, while the attenuation on the ε_{yd-M1} and ε_{yd-M2} disturbance curves enhanced with frequency, it also results in phase shifts. On the contrary, the ε_{yd-M3} disturbance curve shows a phase-frequency characteristic of 0deg in the low-frequency band, especially with a smaller amplitude and phase shift within 22Hz. It indicates that ACPDC tracks and suppresses low-frequency disturbances better than other conventional strategies. Meanwhile, ACPDC has a larger bandwidth range and better dynamic performance against disturbances.

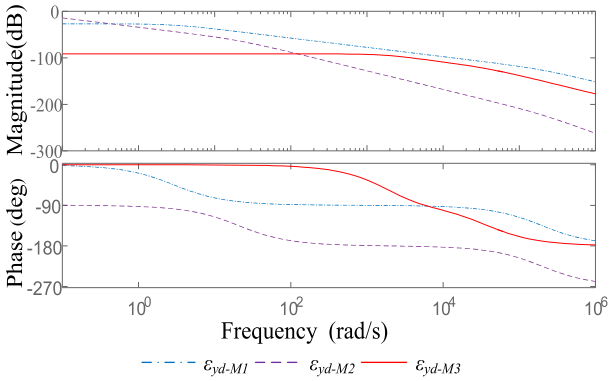

FIGURE 6. The closed-loop characteristic curve of the disturbance component.

TABLE 2. Parameters of PMLSMs.

Parameter	X-axis	Y-axis	Unit
Mover mass	21	4	kg
Continuous force	144	22	N
Peak force	216	88	N
Stator resistance	19.2	12.5	Ω
Inductance	6.47	5.19	mH
EMF constant	52	34.6	V/m/s
Rated current	1.6	1.65	A
Polar distance	0.036	0.015	m

Based on the above CEAM analysis, ACPDC is not only a high-gain controller but also has better dynamic compatibility between multiple axes than conventional strategies. Also, disturbances have less impact on ACPDC. Theoretically, ACPDC improves the contour performances to reduce contour error in both indirect and direct aspects.

IV. EXPERIMENTAL ANALYSIS

A. PREPARATION

The control object of this paper is X-Y linear motor motion platform. To verify the feasibility of ACPDC, experiments are conducted on an X-Y linear motor platform, as shown in Fig. 7. Specifically, both axes include a 0.5μm/pulse grating ruler, a driver using TMS320F28335 as the control chip, and are powered by 24V DC. The interrupt frequency is set to 10 kHz, and drivers exchange data through a serial bus. The position data is collected in real time by the eQEP module and then connected to the monitor through CAN bus. However, it is worth noting that it is more difficult

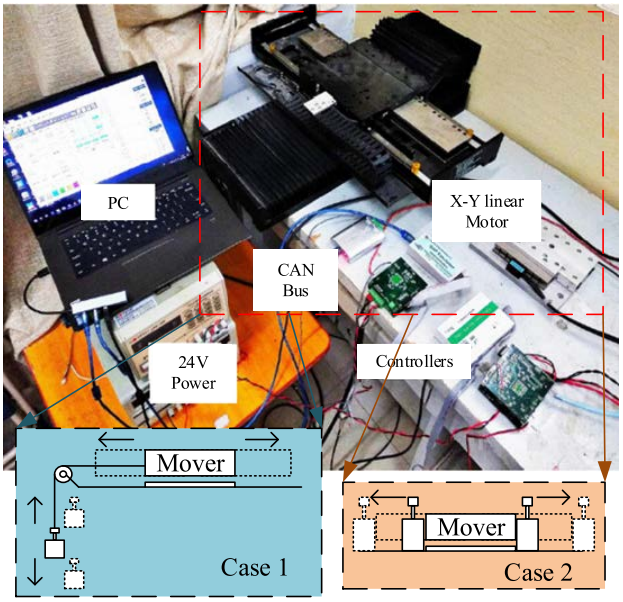

FIGURE 7. Top view of experimental devices.

to coordinate dynamic compatibility between biaxial motors when the biaxial motors parameters are not consistent. So, these experiments use PMLSMs with different parameters are shown in Table 2.

Case 0 (friction disturbance): The running of biaxial motors is only affected by friction disturbances.

Case 1 (continuous disturbance): The X-axis motor is kept constant with Case 0, and the Y-axis motor continuously pulls a 500g weight in a fixed direction on one side.

Case 2 (sudden disturbance): The X-axis motor is kept constant with Case 0, and two 500g weights are respectively placed on each side of the Y-axis motor moving plane.

The following controllers are implemented for comparison:

M1 – PID (indirect method): Biaxial motors run independently with a three-loop cascades P-PI-PI control. The current-loop PI controller parameters are designed by the Siemens optimal tuning method [22], the velocity-loop PI controller parameters are selected based on the oscillation index method [23], and the position-loop P controller parameter is selected according to the principle of $\xi = 1$, $KT = 0.25$ [18].

M2–PID+CCC (direct method): Compared with M1, CCC is introduced into the motion system between two-axes in M2.

M3–ACPDC (Combine indirect method and direct method): The controller proposed in this paper.

Then system performances are evaluated from two aspects, i.e., contour error indexes and uniaxial error indexes.

$$\varepsilon_{rms} = \sqrt{\frac{1}{T}\int |\varepsilon|^2 dt} \tag{43}$$

$$\varepsilon_m = max\{|\varepsilon|\} \tag{44}$$

$$e_{rms-i} = \sqrt{\frac{1}{T}\int |e_i|^2 dt} \tag{45}$$

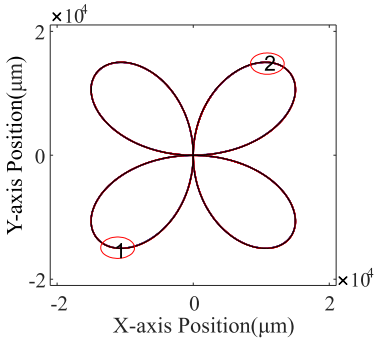

FIGURE 8. The four-leaf clover trajectory.

TABLE 3. Contour indexes under Case 0 & Case 1 & Case 2.

	Case 0		*Case 1*		*Case 2*	
	ε_m	ε_{rms}	ε_m	ε_{rms}	ε_m	ε_{rms}
M1(μm)	18.0	7.45	20.0	9.50	24.5	10.07
M2(μm)	11.5	5.11	14.0	6.51	16.0	7.06
M3(μm)	8.0	1.79	9.0	1.62	7.5	1.97

$$e_{m-i} = max\{|e_i|\} \tag{46}$$

where ε_{rms} and e_{rms-i} are the root mean square values of contour error and uniaxial error, ε_{max} and e_{max-i} are the maximum ab-solute values of contour error and uniaxial error, T denotes the total running time. $i = x, y$, denotes X-axis and Y-axis respectively.

B. FOUR-LEAF CLOVER TRAJECTORY EXPERIMENT

Tracking experiments on large curvature clover trajectories provide a better representation of the controllers' contour performance. The curve function is expressed as

$$\begin{cases} x(t) = qsin(\pi t)sin(0.5\pi t) \\ y(t) = qsin(\pi t)cos(0.5\pi t) \end{cases} \tag{47}$$

where $q = 1.95 \times 104$ (μm). The four-leaf clover trajectory is shown in Fig. 8.

1) CONTOUR PERFORMANCES

Fig. 9 (a) – 9(d) present the motion performances of above controllers tracking the four-leaf clover trajectory, which is only affected by friction disturbance. In Fig. 9(a) and Fig. 9(b), M2 curve basically coincides with M1 curve near corners, while M3 is optimized so that its curve is closest to the Ref curve. In addition, contour error of M2 and M3 in Fig. 9(c) are smaller than that of M1, which proves the effectiveness of the inter-axis controller. And compared with M1 in Table 3, M2 and M3 are decreased by 36.11% and 55.56% in ε_m, reduced by 31.41% and 75.97% in ε_{rms}, respectively.

From Fig. 9(e) – 9(i), M3 curve always keeps the best tracking at corners, despite the Y-axis motor is affected by different types of disturbances. It can be seen that M3 has the best disturbance suppression. These phenomena are supported in Fig. 9(g) and Fig. 9(k). As described in Fig. 9(g) and Fig. 9(k), M3 curve is located at the bottom, followed by M2 curve and M1 curve. As presented in Table 3, relative to M1, ε_m of M2 are decreased by 30.00% and 34.69%, ε_{rms} of M2 are

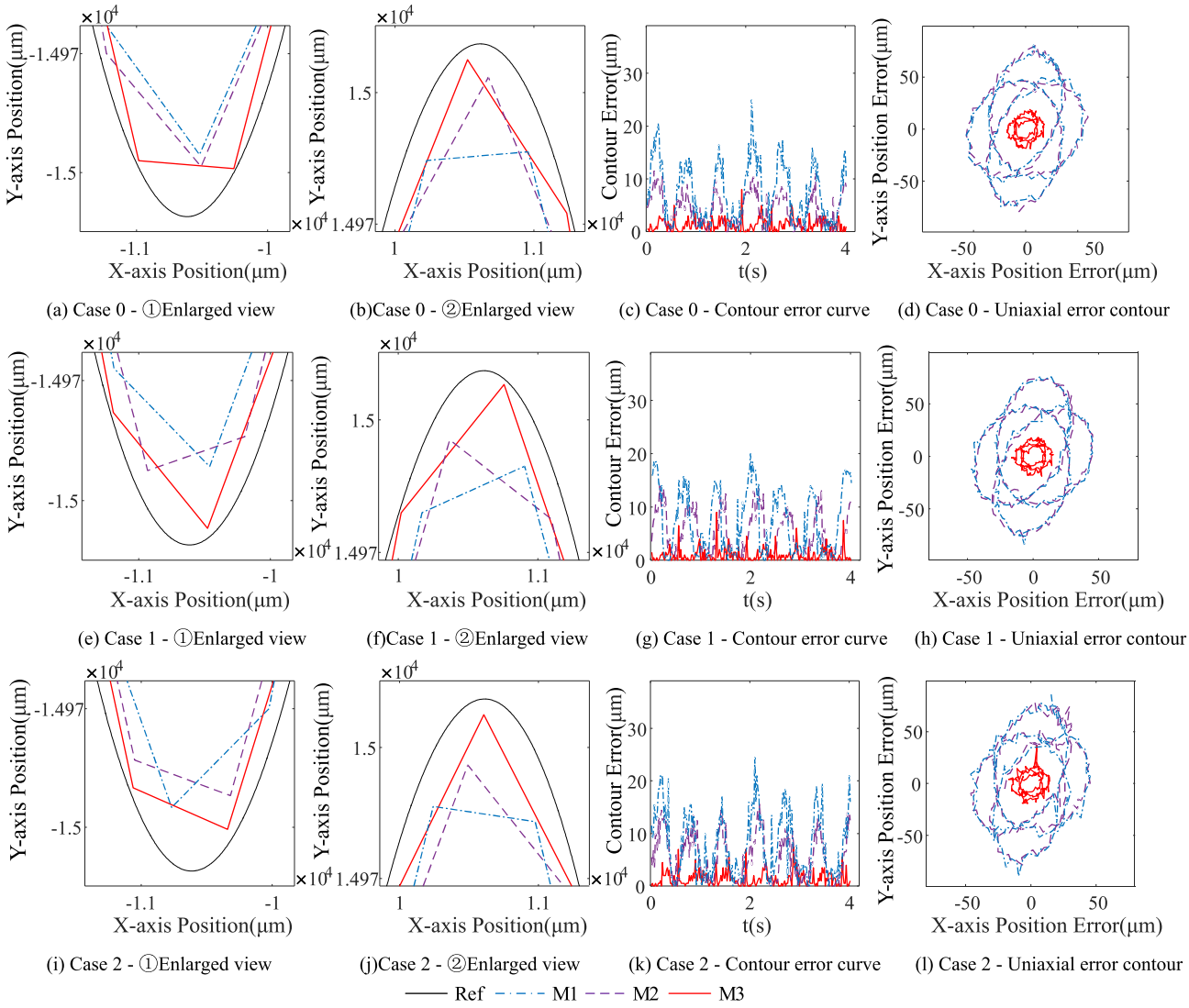

FIGURE 9. Track the four-leaf clover.

down 31.47% and 29.89%. As for ε_m of M3, they reduced by 55.00% and 69.39%, ε_{rms} of M3 are down to 82.95% and 80.43%. The reason for these improvements is that M3 reduces the influence of disturbances by promoting the system robustness compared with M1 and M2. Meanwhile, the dual-channel compensation structure of M3 can obtain more accurate information for ACPDC and thus decrease contour error. In addition, the code running time of M3 is about 31 μs, occupying 31% of interrupt resources, which is about 5% larger than that of M2. Confirmed the possibility of ACPDC implementation.

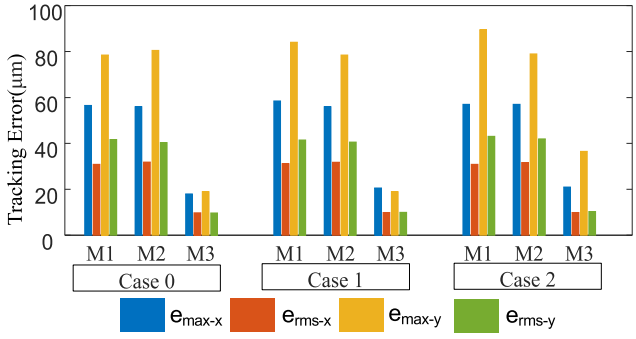

FIGURE 10. The uniaxial error quantization.

2) UNIAXIAL PERFORMANCES

To further verify the different influences of controllers on the uniaxial performances, uniaxial error contour is constructed from two-axis uniaxial error. The smaller the uniaxial error contour is, the better the uniaxial performances are. Meanwhile, the disturbances transmission between biaxial systems can be judged based on the symmetry of uniaxial error contours.

Fig. 9(d), 9(h) and 9(l) respectively depict the uniaxial error contours for different conditions. With different controllers, all three error contours are the four-leaf clover shape. Specifically, M3 presents a standard four-leaf clover contour,

while M1 curve and M2 curve are non-standard, i.e., short on the X-axis and long on the Y-axis. Among them, both the M1 curve and M2 curve are overlap, but M3 curve is the smallest of these contours. In particular, in *Case 2(sudden disturbance)* of Fig. 9(l), the Y-axis error increases sharply due to the sudden force on one side of Y-axis, and M3 still maintains a small error and tracking performance. This phenomenon means that M3 has better uniaxial performances and robustness to reduce the inter-axis trans-mission of disturbances. A similar conclusion can be drawn from Fig. 10, where M3 not only has the minimal uniaxial error but also has the same performance indexes value for both axes. It further proves that the M3 improvements are better than the other two controllers.

V. CONCLUSION

For the motion control in the X-Y linear motor platform, this paper deduced CEAM and designed ACPDC which had improved the contour performance. The main contributions were as followed:

(1) In this paper, the concept of CEAM was deduced and the essence of contour error was discussed. On the one hand, three key factors leading to contour errors can be deduced from CEAM: uniaxial subsystem performance, dynamic compatibility between multiple axes, and disturbances. On the other hand, since all controllers capable of constructing transfer functions can use CEAM to analyze their performances, CEAM was universally applicable. Therefore, it was helpful to subsequent scholars to further analyze the essence of contour error.

(2) Based on the CEAM conclusions and the unified modeling idea, ACPDC was designed by combining the advantages of two aspects. ACPDC was improved the coupling level of the dual-axis system as well as directly improved contour performance. Meanwhile, it was promoted robustness of the system and performance of the uniaxial subsystem, which indirectly reduced contour error.

Through a series of comparison experiments, CEAM was shown to effectively reflect the characteristics of contour control and contour prediction error. Meanwhile, ACPDC not only achieved higher accuracy contour tracking compared with other control strategies, but also enhanced system robustness and uniaxial subsystem performance, which was beneficial to realize optimal contour control.

REFERENCES

[1] B. Li, "Iterative learning and modify adaptive disturbance compensate method for contour control of X-Y table," in *Proc. 33rd Chin. Control Decis. Conf. (CCDC)*, May 2021, pp. 4276–4280, doi: 10.1109/CCDC52312.2021.9602001.

[2] W. Xu, J. Hou, J. Li, C. Yuan, and A. Simeone, "Multi-axis motion control based on time-varying norm optimal cross-coupled iterative learning," *IEEE Access*, vol. 8, pp. 124802–124811, 2020.

[3] R. Wang, F. Man, D. Yan, B. Hu, S. Sun, Q. Chen, and J. Wang, "Research on multi-loop nonlinear control structure and optimization method of PMLSM," *IEEE Access*, vol. 7, pp. 165048–165059, 2019.

[4] M. Fatih Corapsiz and K. Erenturk, "Trajectory tracking control and contouring performance of three-dimensional CNC," *IEEE Trans. Ind. Electron.*, vol. 63, no. 4, pp. 2212–2220, Apr. 2016.

[5] M. Tomizuka, "Zero phase error tracking algorithm for digital control," *ASME Trans. J. Dyn. Syst. Meas. Control*, vol. 109, no. 1, pp. 65–68, Mar. 1987.

[6] B. Zhang, R. Cao, and Z. Hou, "The model-free adaptive cross-coupled control for two-dimensional linear motor," *Trans. Inst. Meas. Control*, vol. 42, no. 5, pp. 1059–1069, Mar. 2020.

[7] Q. Du, Q. Xiong, W. Liu, R. Wang, and W. Huang, "Contour error control of X-Y motion platform based on robust predictive," in *Proc. 13th Int. Symp. Linear Drives Ind. Appl. (LDIA)*, Wuhan, China, Jul. 2021, pp. 1–6.

[8] A. Ghaffari and A. G. Ulsoy, "Component swapping modularity for distributed precision contouring," *IEEE/ASME Trans. Mechatronics*, vol. 22, no. 6, pp. 2625–2632, Dec. 2017.

[9] Y. Koren, "Cross-coupled biaxial computer for manufacturing systems," *ASME J. Dyn. Syst., Meas. Control*, vol. 102, no. 4, pp. 265–272, 1980.

[10] F. F. M. El-Sousy and K. A. Abuhasel, "Nonlinear robust optimal control via adaptive dynamic programming of permanent-magnet linear synchronous motor drive for uncertain two-axis motion control system," *IEEE Trans. Ind. Appl.*, vol. 56, no. 2, pp. 1940–1952, Mar. 2020.

[11] K. L. Barton and A. G. Alleyne, "A cross-coupled iterative learning control design for precision motion control," *IEEE Trans. Control Syst. Technol.*, vol. 16, no. 6, pp. 1218–1231, Nov. 2008.

[12] C. Hu, T. Ou, H. Chang, Y. Zhu, and L. Zhu, "Deep GRU neural network prediction and feedforward compensation for precision multiaxis motion control systems," *IEEE/ASME Trans. Mechatronics*, vol. 25, no. 3, pp. 1377–1388, Jun. 2020.

[13] Y. Koren and C.-C. Lo, "Variable-gain cross-coupling controller for contouring," *CIRP Ann.*, vol. 40, no. 1, pp. 371–374, Jan. 1991.

[14] X. Yang, R. Seethaler, C. Zhan, D. Lu, and W. Zhao, "A model predictive contouring error precompensation method," *IEEE Trans. Ind. Electron.*, vol. 67, no. 5, pp. 4036–4045, May 2020.

[15] J.-H. Chin and T.-C. Lin, "Cross-coupled precompensation method for the contouring accuracy of computer numerically controlled machine tools," *Int. J. Mach. Tools Manuf.*, vol. 37, no. 7, pp. 947–967, Jul. 1997.

[16] R. Shi and Y. Lou, "Three-dimensional contouring control: A task polar coordinate frame approach," *IEEE Access*, vol. 7, pp. 63626–63637, 2019.

[17] B. Xiao, F. Guo, and Q. Wang, "The research of contour error with PID control based-on disturbance observer," in *Proc. 5th World Congr. Intell. Control Autom.*, Hangzhou, China, Jun. 2004, pp. 4563–4567.

[18] T. Shi, X. Zhang, Z. Zhou, and C. Xia, "Precise contour control of biaxial motion system based on MPC," *IEEE J. Emerg. Sel. Topics Power Electron.*, vol. 6, no. 4, pp. 1711–1721, Dec. 2018.

[19] S.-S. Yeh and P.-L. Hsu, "Estimation of the contouring error vector for the cross-coupled control design," *IEEE/ASME Trans. Mechatronics*, vol. 7, no. 1, pp. 44–51, Mar. 2002.

[20] Z. Wang, C. Hu, and Y. Zhu, "Dynamical model based contouring error position-loop feedforward control for multiaxis motion systems," *IEEE Trans. Ind. Informat.*, vol. 15, no. 8, pp. 4686–4695, Aug. 2019.

[21] Z. Gao, "Scaling and bandwidth-parameterization based controller tuning," in *Proc. Amer. Control Conf.*, Denver, CO, USA, Jun. 2003, pp. 4989–4996.

[22] H. Gross, G. Wiegartner, and J. Hamann, *Electrical Feed Drives in Automation: Basics, Computation, Dimensioning*. Hoboken, NJ, USA: Wiley, 2001.

[23] Y. Li, S. Yang, K. Wang, and D. Zeng, "Research on PI controller tuning for VSC-HVDC system," in *Proc. Int. Conf. Adv. Power Syst. Autom. Protection*, Beijing, China, Oct. 2011, pp. 261–264.

RONGKUN WANG was born in Fujian, China. He received the Ph.D. degree in electrical engineering from the Institute of Modern Physics, Chinese Academy of Sciences, in 2013. He is currently a Master Instructor with Huaqiao University. His current research interests include power electronics and power drives, devoting to digital UPS and its parallel technology, the control of the permanent magnet synchronous linear motor, harmonic detection method and three-level active filter, and another innovative research. He is a major participant in the study of major national science and technology projects, Chinese Academy of Sciences directional projects.

ZHIBIN CHEN was born in Fujian, China. He is currently pursuing the master's degree with Huaqiao University. He has worked on the electric drive and power conversion technology.

QUANKAI DU was born in Fujian, China. He received the M.S. degree from the College of Information Science and Engineering, Huaqiao University, Xiamen, Fujian, in 2022.

He has worked on electric drive and power conversion technology.

ZUOCHAO YU was born in Jilin, China. He received the M.S. degree from the College of Information Science and Engineering, Huaqiao University, Xiamen, Fujian, China, in 2021.

He has worked on electric drive and power conversion technology.

WENJIE HUANG was born in Fujian, China. He received the B.S. degree from the College of Marine Engineering, Jimei University, Fujian, in 2020. He is currently pursuing the M.S. degree with the College of Information Science and Engineering, Huaqiao University, Xiamen. He has worked on electric drive and power conversion technology.

XINHUA GUO was born in Fujian, China, in 1977. He graduated from the Nanjing Institute of Technology, Nanjing, China, in 2000. He received the M.S. degree in agricultural electrification and automation from Jiangsu University, Zhenjiang, China, in 2006, and the Ph.D. degree in electrical engineering from the Institute of Electrical Engineering (IEE), Chinese Academy of Sciences (CAS), Beijing, China, in 2010.

He is currently working as a Professor and the Deputy Dean of the College of Information Science and Engineering, Huaqiao University, Xiamen, China. In addition, he was a Research Assistant at IEE, CAS, and worked as an Engineer at the Japanese company TDK, and the American Company Amphenol Assemble Tech (Xiamen) Company Ltd. His current research interests include IGBT packaging technology, PMSMs and their drive control for EVs, and special motors and their drive control. The technical achievements of his research have been industrialized through Zhejiang Semiharv Technology Company Ltd., Taizhou, China, and Xiamen Wise Electrical Technology Company Ltd., Xiamen, respectively, where he is also a Technical Consultant.

Dr. Guo is also the Chairperson of Fujian Power Supply Society.